Journal of Biological Physics 31: 351–363, 2005.
DOI: 10.1007/s10867-005-7286-3

Dynamic Simulation of Active/Inactive Chromatin Domains

JENS ODENHEIMER[1,*], GREGOR KRETH[2] and DIETER W. HEERMANN[1]
[1]*Institut für Theoretische Physik, Universität Heidelberg, Philosophenweg 19, D-69120 Heidelberg, Germany;* [2]*Kirchhoff-Institut für Physik, Universität Heidelberg, Im Neuenheimer Feld 227, D-69120 Heidelberg, Germany*
*(*Author for correspondence, e-mail: j.odenheimer@tphys.uni-heidelberg.de)*

Abstract. In the present study a model for the compactification of the 30 nm chromatin fibre into higher order structures is suggested. The idea is that basically every condensing agent (HMG/SAR, HP1, cohesin, condensin, DNA–DNA interaction . . .) can be modeled as an effective attractive potential of specific chain segments. This way the formation of individual 1 Mbp sized rosettes from a linear chain could be observed. We analyse how the size of these rosettes depends on the number of attractive segments and on the segment length. It turns out that 8–20 attractive segments per 1 Mbp domain produces rosettes of 300–800 nm in diameter. Furthermore, our results show that the size of the rosettes is relatively insensitive to the segment length.

Key words: chromatin structure, simulation, condensing agents, rosette structure, virtual microscopy, molecular dynamics, modeling

1. Introduction

The structure formation of chromatin is studied on many different scales [1]. Interesting properties can already be obtained from models of the formation of the 30 nm fibre [2–7]. Chromatin structures beyond the level of the linear array of nucleosomes play an essential role in gene regulation, repair processes and pathogenic rearrangements in eukaryotes. Changes in functional activity are assumed to be tightly coupled to changes in the chromatin structure. Thus, a full understanding of genome function is not possible without detailed investigations of the functional chromatin structure and its control, requiring appropriate tools for quantitative analysis.

The exact details of the 3D folding of the chromatin fibre of a chromosome are still controversial. Experiments are highly difficult due to the following limitations. Aggregation is promoted by the high cellular concentration and charge of chromosomal material. Furthermore, many structures are smaller than the resolution of the light microscope (roughly 200 nm) and therefore can only be seen by electron microscopy, which in turn causes problems associated with preserving structure and recognition of the 3D folding of specific chromatin structures.

It is generally agreed upon that in eukaryotes the double helix is coiled locally around nucleosomes and globally into distinct nuclear territories [8]. The levels in between are still under discussion [9]. There are several models for the different stages of compactification: (i) structures, in which strings are coiled into solenoids (of roughly 30 nm diameter) or zig-zag tubes [2], which in turn again form higher-order structures [10]; (ii) loops of about 50–150 kbp which are attached to the peripheral lamina or other internal structures, such as skeletons/scaffolds [11] or factories [12]; and (iii) combinations of the above, such as helical coils and radial loops [13] or helical coils and random folding [14].

To investigate the folding and accessibility of virtual active/inactive chromatin domains within the nuclear volume, our model assumes attractive sites at some locations along the chain. The results of our simulation favour the 'Multi Loop Subcompartment' (MLS) model developed in the group of J. Langowski [15,16] for the overall structure of chromosome territories.

According to the MLS model, the experimentally observed focal structure of chromosomes (for an overview see [8, 17]) is described by rosettes of several 100 kbp loops assuming a 30 nm chromatin fibre. Adjacent rosettes are connected by chromatin linker segments with the same DNA content as one loop. Approaches based on the isochore model also predict the formation of rosettes of about 1 Mbp [18].

It has not yet been understood how these rosettes form dynamically. We have developed a model that not only shows that the higher order structures formed are indeed rosettes, but also explains the formation process and predicts quantitative results for certain quantities of interest such as formation time and rosette diameter. Finally, the model predictions will be compared with experimental light microscopic data.

2. The Polymer Model

In this work the continuous backbone mass model [19] is used. The model interpolates between the united atom model and the bead-spring model. In contrast to these two models it uses non-spherical force fields for the non-bonded interaction. The main idea of this approach with a more general form of the force field is to generalise the united atom model in a way that larger atom groups are combined to one construction unit, but the possible anisotropy of these groups is still taken into account. The simplest anisotropic geometrical object one can think of is an ellipsoid of rotational symmetric form and thus it is considered as the interaction volume of the chemical sequences in our model.

As one wants the force field to degenerate into a sphere with increasing distance, we use a confocal force field inside this interaction volume:

$$\mathcal{H}_{\text{inter}} = V_{\text{abs}}\left(\frac{d_1^{(p)} + d_2^{(p)}}{2} - c\right), \tag{1}$$

where $d_1^{(p)}$ and $d_2^{(p)}$ denote the distance of the point $\mathbf{p}$ to the focal points of the ellipsoid and V_{abs} is the absolute potential. For convenience we use only a repulsive part

$$V_{\text{abs}}(r) \sim r^{-6}. \tag{2}$$

The mass of the building units is distributed between the focal points of the ellipsoids in the hard core region of the confocal potential.

The main ingredient of the model is the mass matrix of our rod-chains. In order to construct it, we must first calculate the Lagrangian of a single rod $\mathcal{L}_i = T_i - V_i$ with the kinetic energy T_i and the potential energy V_i. The subindex i marks the position of the rods in the chain. This one-dimensional homogeneous rod i has length l_i starting at $\vec{a}_i$ and ending at $\vec{b}_i$. If we suppose that the rods all have the same mass m and that the velocity of the rod mass scales linearly with the position between the boundaries of the rod, the kinetic energy can be written as

$$\begin{aligned} T_i &= \frac{1}{2}\int_0^{l_i} \frac{m}{l_i}\left(\frac{(l_i - x)\dot{\vec{a}}_i + x\dot{\vec{b}}_i}{l_i}\right)^2 dx \\ &= \frac{1}{6}m\left(\dot{\vec{a}}_i^2 + \dot{\vec{a}}_i\dot{\vec{b}}_i + \dot{\vec{b}}_i^2\right). \end{aligned}$$

Adding the single terms of the rods building the chain, we get the Lagrangian $\mathcal{L}$ of the whole rod-chain. The equations of motion of the chain can be calculated from the Lagrange equations of the second kind. Since the equations of motion separate in each direction, we have only to solve three tridiagonal $(N+1)\times(N+1)$ matrices per chain which consist of N rods per time step of the form

$$\mathbf{W}\ddot{\vec{x}} = \vec{F} \tag{3}$$

$$\frac{m}{6}\begin{pmatrix} 2 & 1 & 0 & 0 & \dots \\ 1 & 4 & 1 & 0 & \dots \\ 0 & 1 & 4 & 1 & \dots \\ \vdots & \vdots & \vdots & \vdots & \ddots \end{pmatrix}\begin{pmatrix} \ddot{x}_0 \\ \ddot{x}_1 \\ \ddot{x}_2 \\ \vdots \end{pmatrix} = \begin{pmatrix} F_{10} \\ F_{11} + F_{21} \\ F_{22} + F_{32} \\ \vdots \end{pmatrix} \tag{4}$$

with the force F_{ij} on the coordinate j of the flexible point i of the chain

$$F_{ij} = -\frac{\partial V_i}{\partial j} \tag{5}$$

and $\ddot{x}_i$ denoting the accelerations of the flexible points of the chain. The flexible points are the link points of the ellipsoids and the end points of the rod-chain. The sub-indices mark the positions in the chain: 0 and $N+1$ are the end-points of the chain and the numbers between them denote the linking points of rods in the chain.

The bonded interactions between neighboring units are given by harmonic length and angle potentials:

$$\mathcal{H}_{\text{bond}} = \frac{1}{2}k(r - r_0)^2 \tag{6}$$

$$\mathcal{H}_{\text{angle}} = \frac{1}{2}k_\theta(\cos\theta - \cos\theta_0)^2 \tag{7}$$

with bond length r and bending angle θ. Here r_0 and θ_0 denote the mean values.

3. The Biological Model

The genome content of a typical human chromosome is on the order of several hundred Mega base-pairs (e.g. 245 Mbp for Chromosome 1). To handle this amount of data on a computer, course-graining is mandatory. On a large scale, one identifies a coiled state of a chromatin fibre as a 1 Mbp bead (Figure 1). Experimental data yield a diameter of a 1 Mbp domain of about 300–800 nm [17]. The aim of this analysis will be to see whether computer simulations of chromatin fibres in interphase yield the known size and assumed structure of such a coil.

On a more detailed level it is interesting to see the inner structure of such a coil. For a pure 30 nm chromatin fibre one assumes there are approximately 40 segments of about 30 kbp per bead. One instance of the model would be the '10 loop model', where the segments form a rosette of 10 loops. Each loop consists of 120 kbp, so that each segment has 30 kbp. The 10 loop domains are interconnected by 120 kbp linkers. Thus, among every four segments there are believed to be attraction sites which couple the segments and thus lead to the formation of a non-random structure. The MLS model and simulations thereof assume a rosette structure from considerations of the bead diameter and weight. It considers the attractive sites to be connected in the centre of the rosette at the base segments of the loops.

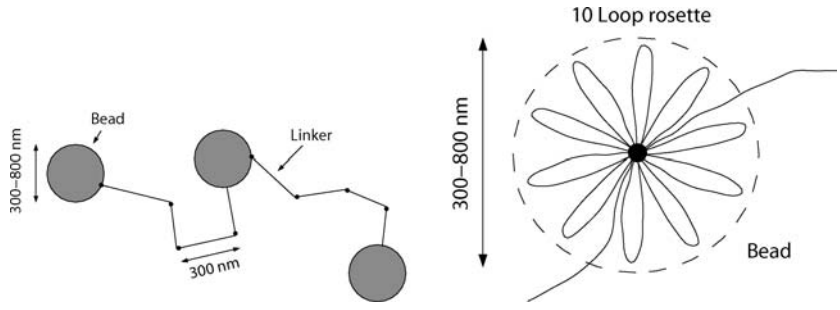

Figure 1. Left: Course-grained model of a chromosome. A typical bead is about 300–800 nm in diameter; the linker segment length is around 300 nm and consists of 30 kbp. Chromosome 1 has approximately 245 such coils. *Right:* Detailed structure of a blob. The 10 loop model suggests a rosette-like structure.

Our model is more general than the MLS-model. We want to look into the formation of any possible higher order structure by starting out with a linear chain. This chain has repulsive and attractive segments. The attractive segments correspond to that part of the chromatin fibre which is affected by some condensing agent. We model the chain such that rosette formation is possible, but not a priori assumed and compulsory. Furthermore, we believe it to be too restrictive not to allow the breaking up of bonds between attraction sites. Therefore, we assume a Lennard-Jones potential. Since there is no reliable data for the Kuhn length of the 30 nm fibre, we simulate the two extreme cases (150 and 300 nm [20]) and see whether there are any significant differences in the results of the interesting observables.

The idea of having attractive elements is quite common in biology. For example the polymerization of microtubules in which tubulin dimers are able to polymerise only if they are first complexed with GTP. Similarly, the pre-replication complexes, that triggers initiation of DNA replication, must first complex with ATP in order to recognize and bind to vacant origins (that work as receptors) in the DNA double helix [21]. The assumption of attractive sites in our case is also biologically justified. For G/Q-R bands, one has shown that HMG/SAR binding proteins act as mediators of attraction [22, 23]. For hetero/euchromatin, the HP1 protein has been associated with chromatin linking [24, 25]. Furthermore, cohesin and condensin play a crucial role in chromosome compaction [11, 26]. The type of condensing agent is not our primary concern, though. Our model also holds if the attraction is mediated by DNA–DNA interaction [27, 28]. Thus, we do not claim that the formation of higher order structures can only occur with a certain type of condensing agent, but rather we look at the general aspect of all agents, namely that they make a certain part of the chromatin fibre effectively attractive.

Our model extracts the underlying idea in every case, namely that the chromatin fibre can be modeled as a multiblock copolymer. Whether you associate the different polymer blocks with GC rich and AT rich regions [18] or with other chromatin characteristics is not of primary importance for our model. A multiblock copolymer containing two alternately located types of blocks can form a single-chain string of loop clusters called micelles [29]. A micelle consists of a certain number of loops. The ends of the loops formed by blocks of one type are located close to each other.

Micellar structures have been thoroughly studied for diblock copolymers and ionomers [30, 31]. Large multiblock copolymers form single-chain micelles, and small diblock copolymers form multichain micelles. The formation of loops and their organisation into micelles are basically entropically unfavorable processes, because the number of possible polymer conformations decreases, but it occurs nonetheless in multiblock copolymers because of the energetically favorable processes of repulsion between unlike monomer units and/or attraction between like monomer units [32, 33]. In an aqueous solution, for example, this means that the hydrophobic parts of the copolymer concentrate in the centre of the micelle and the hydrophilic parts form the loops.

With the abstraction to multiblock copolymers, this leads us to the parameters and potentials we use in our simulations:

- Segment diameter: 30 nm.
- Segment length: two different simulations
  (a) 30 kbp = 300 nm each,
  (b) 15 kbp = 150 nm each.
- The harmonic bond potential is taken to be

$$U_{\mathrm{s}}(l) = \frac{kT}{2\delta^2}\left(l - l_0\right)^2 \tag{8}$$

  with $\delta = 0.1$ and $l_0 = 300$ nm at 310.15 K.
- The angular and torsional potentials are taken to be 0. On this scale the chain is flexible.
- The repulsive segment potential is

$$U_{\mathrm{rep}}(r) = \epsilon\left(\frac{\sigma}{r - r_{\mathrm{segment}}}\right)^6 \tag{9}$$

  with $\epsilon = 0.14 k_{\mathrm{b}}T$ at body temperature, $\sigma = 15$ nm and $r_{\mathrm{segment}} = 15$ nm being the fibre radius.
- Cutoff for the repulsive potential is $r_{\mathrm{c}} = 8$ nm (after the 30 nm fibre diameter).
- The attractive segment potential

$$U_{\mathrm{attr}}(r) = 4\epsilon\left[\left(\frac{\sigma}{r - r_{\mathrm{segment}}}\right)^{12} - \left(\frac{\sigma}{r - r_{\mathrm{segment}}}\right)^{6}\right] \tag{10}$$

  with $\epsilon = 7 k_{\mathrm{b}}T$ at body temperature and $\sigma = 30$ nm.
- Cutoff for the Lennard–Jones potential is $r_{\mathrm{c}} = 80$ nm (after the 30 nm fibre diameter).

4. Simulation Results

We look into the structure formation of a 1 Mbp domain in interphase. The final structure turns out to always be a rosette. We take two non-reactive linkers at the end and an attraction site after n successive segments. The number n of segments is the varying parameter. The diameter of the rosettes will be analysed as a function of this parameter. We get a starting configuration as shown in Figure 2. The attraction agents are marked as spheres. The attractive sites are of the same length as the repulsive ones. The intermediate and final structures are shown in the same figure.

In Figure 3, we show the average formation time of a rosette. Plotted are the minimum, average and maximum distance of the attractive Lennard–Jones segments. The minimum distance drops almost instantly, implying that two attractive segments immediately find each other. After an initial rise, which is due to the random and hence mostly nonphysical starting configuration, the maximum distance decays over a time of about 10 000 MD-Steps. After this amount of time the distance

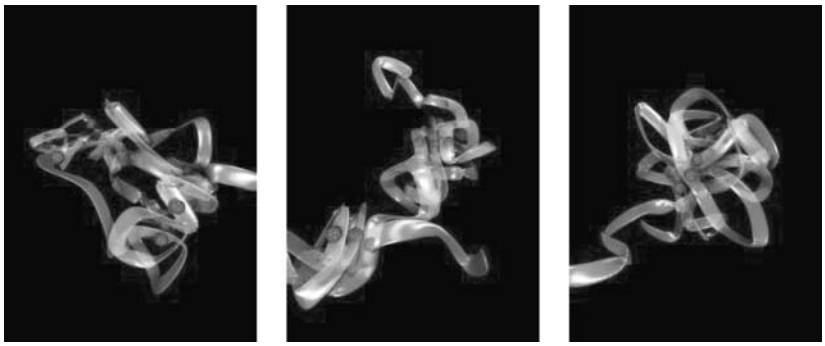

Figure 2. Left: We see the starting configuration of a 60 segment chromatin fibre. The spheres represent the condensing agents. *Center:* An intermediary configuration. This state of mainly two clusters of approximately equal size turns out to be a metastable state. *Right:* In the final state all attractive segments are concentrated in the centre. A rosette has formed.

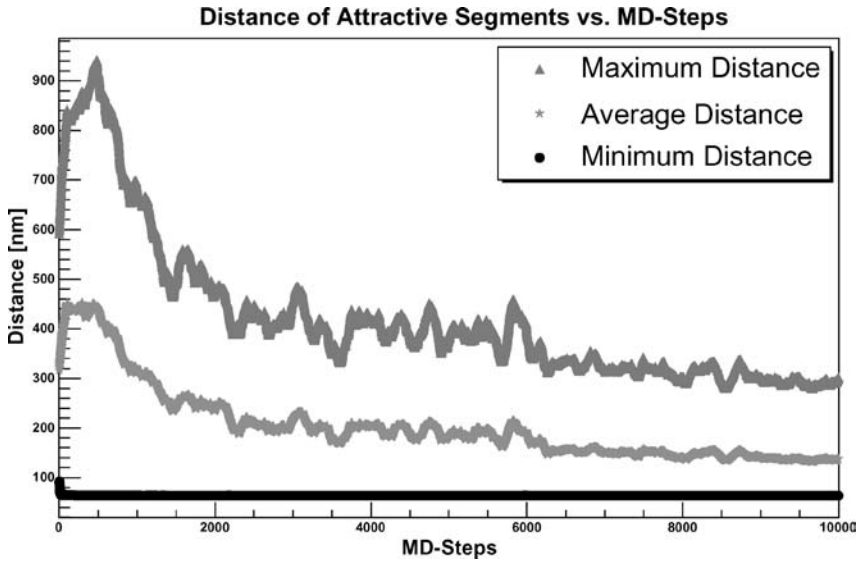

Figure 3. Shown is the average formation time of a rosette. From the minimal distance we conclude that two segments 'snap' very fast. After about 10 000 MD steps, a complete rosette is formed.

drops no more. Hence all attractive segments have found each other. Therefore the fully equilibrated structure is shown to be a rosette. With the given parameters of ϵ and σ, we observe a formation time of about 48 ms. Note that this is the formation time based on the simulation of a single rosette. It remains to be seen how this time changes when a larger region is analysed.

A crucial question is obviously how many attractive sites are required to form rosettes of the size observed under a microscope. In order to analyse this, we have

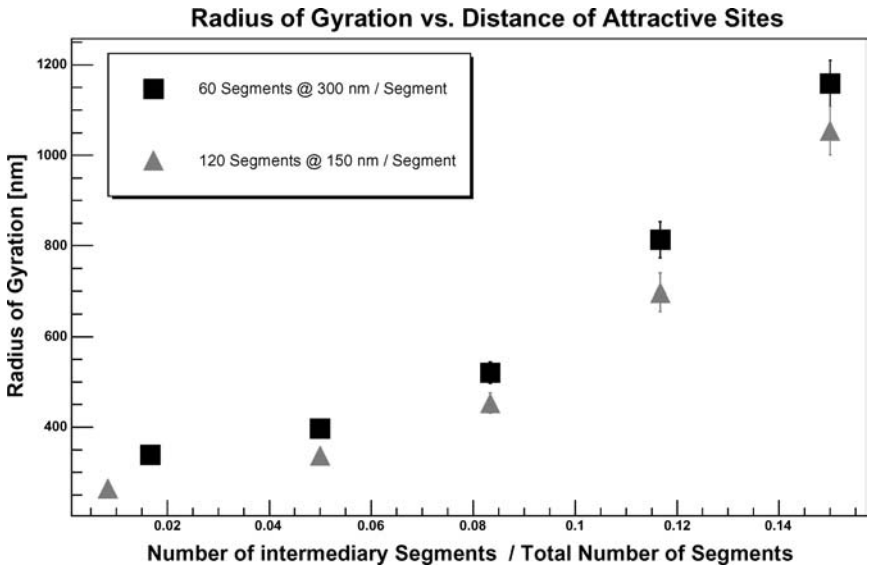

Figure 4. The diameter of the rosettes depends on the number of attractive sites. The different Kuhn lengths are only of minor importance.

performed simulations for regular patterns of attractive/repulsive segments. We are aware of the fact that a regular pattern is a severe restriction, but it allows us to draw conclusions with less statistics than for random patterns. Furthermore, it should provide a first insight whether rosettes of the required size are possible in the first place.

In Figure 4, we have plotted the radii of gyration for different regular patterns and different Kuhn lengths. The circles represent the 300 nm segment and the squares the 150 nm segment. This is the accepted range for the Kuhn length of the 30 nm fibre. Thus, by taking the two extreme cases we can study the effect of the stiffness of the chain.

The following patterns have been simulated:

1. 300 nm segment:
   - attractive site every segment
   - attractive sites every 3 segments
   - attractive sites every 5 segments
   - attractive sites every 7 segments
   - attractive sites every 9 segments
2. 150 nm segment:
   - attractive site every segment
   - attractive sites every 6 segments
   - attractive sites every 10 segments
   - attractive sites every 14 segments
   - attractive sites every 18 segments

Table I. Loop sizes for different Kuhn lengths

L_{segment}	$N_{\text{attractive}}$	$N_{\text{intermediary}}$	Loop size
300	7–19	7–3	90–210 kbp
150	7–19	14–6	90–210 kbp

As expected we see a clear increase in the radius of gyration with larger loop sizes. For example, for the 300 nm Kuhn length with a loop size of 7 segments (with a total number of 60 segments per rosette we get a ratio of about 0.12), we obtain a radius of gyration of about 800 nm. We will see later that the radius of gyration corresponds very well to the actual diameter. So for a given (experimental [34]) diameter of 300–800 nm we need 7–19 attractive segments, i.e. every third to every eighth segment, for the 300 nm Kuhn segment. Therefore we have loop sizes of 90–210 kbp (i.e. 3–7 segments), with the optimal value around 120 kbp (four segments) per loop. This result is well supported by the literature [12, 35–37]. The different Kuhn lengths produce only a slight difference in the diameter. The main parameter is clearly the number of attractive segments. Table I illustrates the optimal values for rosette diameters of 300–800 nm. L_{segment} indicates the segment length, $N_{\text{attractive}}$ the total number of attractive segments per rosette and $N_{\text{intermediary}}$ the number of repulsive segments between the attractive ones.

Plotting the two-dimensional average monomer concentration yields Figure 5. The average is taken from 10 000 uncorrelated configurations. The data in the figure corresponds to the 300 nm segment with an attractive site every five segments. We see that the 1 Mbp domain has a diameter of about 600 nm. This corresponds exactly to the radius of gyration. Hence the radius of gyration is a very good indicator of the actual diameter. It is clear that the centre cannot be the most likely position for the monomers since we have excluded volume. Furthermore, the attractive sites are all within each other's potential minimum so that we have a smeared-out centre where the attractive sites are. Moving farther out to the periphery, we observe a higher monomer concentration. This is the region dominated by the loops.

To compare the modeled configurations with the outcome of light microscopy, in Figure 5 (top), projections of virtual microscopy image data stacks are shown. This approach consisted of a digitisation of the 30 nm thick segments (about 10 points per 30 kbp sized segment were digitised) by a grid of $4.9 \times 4.9 \times 10.5$ nm voxel spacing and a convolution of the digitised stacks with a measured confocal point spread function (PSF) (with a full width at half maximum (FWHM): FWHMx = 279 nm, FWHMy = 254 nm, FWHMz = 642 nm).

To further narrow the number of possible attraction sites per 1 Mbp domain we plot the spatial versus the genomic distance in Figure 6. The data are fitted against the power law $y = ax^b$ for the 300 nm/segment chains, where y is the spatial distance, x the genomic distance and a and b the fit parameters. The results of the fits are shown in Table II.

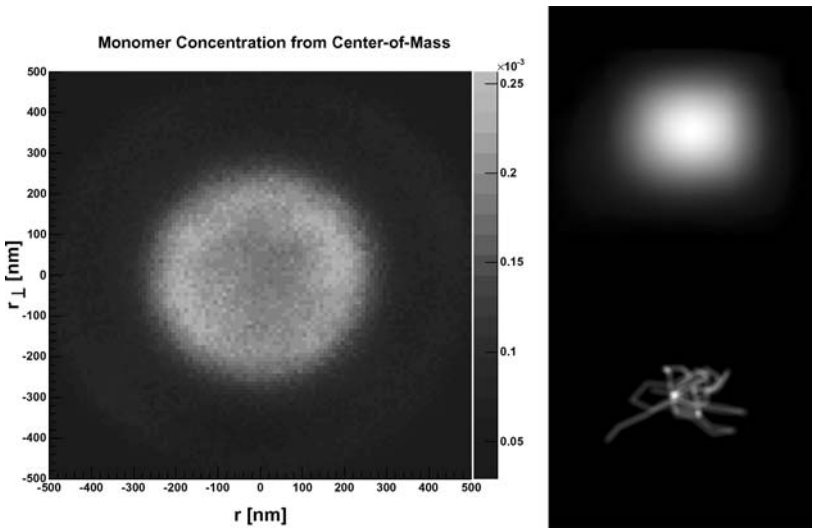

Figure 5. Left: 2-dimensional histogram of the projection of the average monomer concentration of a rosette with a diameter of about 600 nm. The grey values are the respective normalized probabilities. *Right:* Projections of virtual microscopy image data stacks of one simulated rosette (before convolution with a measured confocal point spread function (bottom) and after convolution (top)).

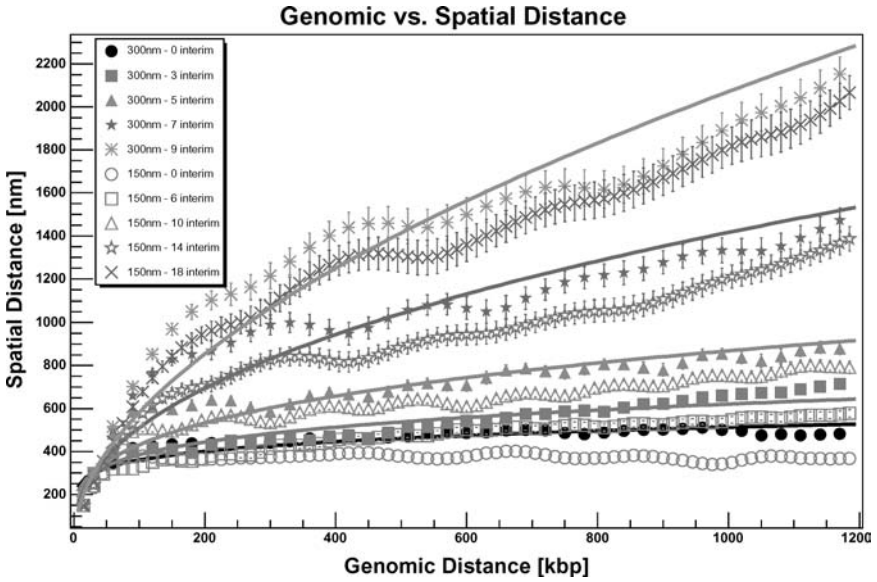

Figure 6. Shown is the spatial vs. the genomic distance of a 1 Mbp domain. The exponents yielded by the fits clearly favour about 11 attractive sites per 1 Mbp domain. The oscillations in the data are due to the rosette nature of the 1 Mbp domain.

Table II. Fit parameters for $y = ax^b$

$N_{\text{attractive}}$	a	b
5	177.74 ± 0.86	0.1535 ± 0.0014
7	148.05 ± 0.76	0.2075 ± 0.0015
11	106.97 ± 0.68	0.3031 ± 0.0019
19	66.60 ± 0.53	0.4425 ± 0.0024
50	46.06 ± 0.38	0.5509 ± 0.0024

The exponents yielded by the fits show that about 11–12 attractive segments per 1 Mbp domain are needed in order to exhibit a non-random walk behaviour with an exponent of about 1/3. Therefore, the number of attractive sites suggested by the evaluation of the diameter, namely about 11 per 1 Mbp domain, is consistent with the number proposed by the exponent. The exponent of 0.32 ± 0.02 was obtained by Münkel [15] based on the experiments by Yokota *et al.* [38] for genomic distances of several Mbps. The parameter range yielded by our simulation results is therefore in good agreement with experiment.

5. Discussion

In summary, we have found that our model, which uses only a linear chain with attractive and repulsive segments, describes the formation of rosettes without any further constraints. It turns out that the different Kuhn lengths are only of minor importance. The main parameter is the number of attractive segments. The best candidates for producing rosettes with a diameter of 300–800 nm are: every third to eighth segment attractive for the 300 nm Kuhn length and every sixth to sixteenth segment attractive for the corresponding 150 nm Kuhn length, thus producing loop sizes of 90–210 kbp. Furthermore, we have shown that the radius of gyration is a convenient observable for the actual diameter. Plotting the spatial versus genomic distance of our 1 Mbp rosettes narrowed the parameter range even more and showed that we are in good agreement with experiment. Thus the optimal size loop predicted by our model is about 120 kbp, yielding an exponent of 0.3031 ± 0.0019, which is in good agreement with the literature.

Acknowledgement

We would like to thank C. Cremer for stimulation and support and T. Cremer, K. Rippe and J. Langowski for helpful discussions.

References

1. Schiessel, H.: The Physics of Chromatin, *J. Phys.: Cond. Matter* **15** (2003), 699–774.

2. Wedemann, G. and Langowski, J.: Computer Simulation of the 30-Nanometer Chromatin Fiber, *Biophys. J.* **82** (2002), 2847–2859.
3. Beard, D.A. and Schlick, T.: Computational Modeling Predicts the Structure and Dynamics of Chromatin Fiber, *Structure* **9** (2001), 105–114.
4. Bednar, J., Horowitz, R.A., Grigoryev, S.A., Carruthers, L.M., Hansen, J.C., Koster, A.J. and Woodcock, C.L.: Nucleosomes, Linker DNA, and Linker Histone Form a Unique Structural Motif that Directs the Higher-Order Folding and Compaction of Chromatin, *Proc. Natl. Acad. Sci. USA* **95** (1998), 14173–14178.
5. Schiessel, H.: How Short-Ranged Electrostatics Controls the Chromatin Structure on much Larger Scales, *Europhys. Lett.* **58** (2002), 140–146.
6. Schiessel, H.: DNA Folding: Structural and Mechanical Properties of the Two-Angle Model for chromatin, *Biophys. J.* **80** (2001), 1940–1956.
7. Schiessel, H.: Theory and Computer Modeling of the 30 nm Chromatin Fiber, *New Compr. Biochem.* **39** (2004), 397–420.
8. Cremer, T. and Cremer, C.: Chromosome Territories, Nuclear Architecture and Gene Regulation in Mammalian Cells, *Nat. Rev. Genet.* **2** (2001), 292–301.
9. Cook, P.R.: *Principles of Nuclear Structure and Function*, Wiley, New York, 2001.
10. Sedat, J. and Manuelidis, L.: A Direct Approach to the Structure of Eukaryotic Chromosomes, *Cold Spring Harb. Symp. Quant. Biol.* **42** (1978), 331–350.
11. Maeshima, K. and Laemmli, U.K.: A Two-Step Scaffolding Model for Mitotic Chromosome Assembly, *Dev. Cell* **4** (2003), 467–480.
12. Cook, P.R.: A Chromomeric Model for Nuclear and Chromosome Structure, *J. Cell Sci.* **108** (1995), 2927–2935.
13. Manuelidis, L.: A View of Interphase Chromosomes, *Science* **250** (1990), 1533–1540.
14. Li, G., Sudlow, G. and Belmont, A.S.: Interphase Cell Cycle Dynamics of a Late-Replicating, Heterochromatic Homogeneously Staining Region: Precise Choreography of Condensation/Decondensation and Nuclear Positioning, *J. Cell Biol.* **140** (1998), 975–989.
15. Münkel, C. and Langowski, J.: Chromosome Structure Predicted by a Polymer Model, *Phys. Rev. E* **57** (1998), 5888–5896.
16. Münkel, C., Eils, R., Dietzel, S., Zink, D., Mehring, C., Wedemann, G., Cremer, T. and Langowski, J.: Compartmentalization of Interphase Chromosomes Observed in Simulation and Experiment, *J. Mol. Biol.* **285** (1999), 1053–1065.
17. Cremer, T., Kreth, G., Koester, H., Fink, R.H.A., Heintzmann, R., Cremer, M., Solovei, I., Zink, D. and Cremer, C.: Chromosome Territories, Interchromatin Domain Compartment and Nuclear Matrix: An Integrated View of the Functional Nuclear Architecture, *Crit. Rev. Eukaryotic Gene Expr.* **12** (2000), 179–212.
18. Ostashevsky, J.: A Polymer Model for the Structural Organization of Chromatin Loops and Minibands in Interphase Chromosomes, *Mol. Biol. Cell* **9** (1998), 3031–3040.
19. Schöppe, G. and Heermann, D.W.: Alternative Off-latice Model with Continuous Backbone Mass for Polymers, *Phys. Rev. E.* **59** (1999), 636–641.
20. Rippe, K.: Making Contacts on a Nucleic Acid Polymer, *TRENDS Biochem. Sci.* **26** (2001), 733–740.
21. Matsson, L.: DNA Replication and Cell Cycle Progression Regulated by Long Range Interaction Between Protein Complexes Bound to DNA, *J. Biol. Phys.* **27** (2001), 329–359.
22. Girard, F., Bello, B., Laemmli, U.K. and Gehring, W.J.: In Vivo Analysis of Scaffold-Associated Regions in Drosophila: A Synthetic High-Affinity SAR Binding Protein Suppresses Position Effect Variegation, *EMBO J.* **17** (1998), 2079– 2085.
23. Hart, C.M. and Laemmli, U.K.: Facilitation of Chromatin Dynamics by SARs, *Curr. Opin. Genet. Dev.* **8** (1998), 519–525.

24. Maison, C. and Almouzni, G.: Hp1 and the Dynamics of Chromatin Maintenance, *Nat. Rev. Mol. Cell Biol.* **5** (2004), 296–305.
25. Ishii, K. and Laemmli, U.K.: Structural and Dynamic Functions Establish Chromatin Domains, *Mol. Cell* **11** (2003), 237–248.
26. Blat, Y. and Kleckner, N.: Cohesins Bind to Preferential Sites Along Yeast Chromosome III, with Differential Regulation along Arms Versus the Centric Region, *Cell* **98** (1999), 249–259.
27. Cherstvy, A.G., Kornyshev, A.A. and Leikin, S.: Temperature-Dependent DNA Condensation Triggered by Rearrangement of Adsorbed Cations, *J. Phys. Chem. B* **106** (2002), 13362–13369.
28. Cherstvy, A.G., Kornyshev, A.A. and Leikin, S.: Torsional Deformation of Double Helix in Interaction and Aggregation of DNA, *J. Phys. Chem. B* **108** (2004), 6508–6518.
29. Halperin, A.: On the Collapse of Multiblock Copolymers, *Macromolecules* **24** (1991), 1418–1419.
30. Semenov, A.N., Joanny, J.-F. and Khokhlov, A.R.: Associating Polymers: Equilibrium and Linear Viscoelasticity, *Macromolecules* **28** (1995), 1066–1075.
31. Semenov, A.N., Nyrkova, I.A. and Khokhlov, A.R.: *Ionomers: Characterization, Theory and Applications, Chapter Statistics and Dynamic of Ionomer Systems*, CRC Press, Boca Raton, FL, 1996, pp. 251–279.
32. De Gennes, P.-G.: *Scaling Concepts in Polymer Physics*, Cornell University Press, Ithaca, 1979.
33. Grosberg, A.Y. and Khokhlov, A.R.: *Statistical Physics of Macromolecules*, AIP Press, New York, 1994.
34. Bornfleth, H., Edelmann, P., Zink, D., Cremer, T. and Cremer, C.: Quantitative Motion Analysis of Subchromosomal Foci in Living Cells Using Four-Dimensional Microscopy, *Biophys. J.* **77** (1999), 2871–2886.
35. Wolffe, A.: *Chromatin: Structure and Function*, Academic Press Inc., San Diego, 2nd edn., 1995.
36. Saitoh, Y. and Laemmli, U.K.: Metaphase Chromosome Structure: Bands Arise from a Differential Folding Path of the Highly AT-rich Scaffold, *Cell* **76** (1994), 609–622.
37. Bickmore, W.A. and Oghene, K.: Visualizing the Spatial Relationships Between Defined DNA Sequences and the Axial Region of Extracted Metaphase Chromosomes, *Cell* **84** (1996), 95–104.
38. Yokota, H., van den Engh, G., Hearst, J.E., Sachs, R.K. and Trask, B.J.: Evidence for the Organization of Chromatin in Megabase Pair-Sized Loops Arranged Along a Random Walk Path in the Human G_0/G_1 Interphase Nucleus, *J. Cell Biol.* **130** (1995), 1239–1249.